Iraqi Journal of Science, 2025, Vol. 66, No. 12, pp: 5831- 5840
DOI: 10.24996/ijs.2025.66.12.44

ISSN: 0067-2904

Integration of Remote Sensing and GIS for Mapping of Land Cover Change due to Flash Floods in Simangulampe, North Sumatra, Indonesia

Wikan Jaya Prihantarto[1]*, Eva Purnamasari[1], Muhammad Ismail[1] Sri Kandi Putri [1] Erisa Waspadi Putri[2] Maulana Yudinugroho[3]

[1]*Departement of Geography, Faculty of Social Science, Universitas Negeri Padang, Padang, Indonesia*
[2]*Department of Forestry, Faculty of Forestry, Universitas Tanjungpura, Pontianak, Indonesia*
[3]*Department of Geomatic Engineering, Faculty of Technology Mineral, Universitas Pembangunan Nasional Veteran, Yogyakarta , Indonesia*

Received: 14/6/2024 Accepted: 3/12/2024 Published: 30/12/2025

Abstract

Flash floods hit Simangulampe Village, North Sumatra, Indonesia, on December 1st, 2023. This incident resulted in loss of life, material damage, and environmental change around impacted areas. This study aims to map land cover changes due to flash floods and analyze the flash flood source area using remote sensing data integrated with GIS. Mapping was conducted using two Planet Scope images recorded before and after the disaster. The multispectral classification was used to obtain land cover maps from these images, and both of them were analyzed using the overlay method. 30 m SRTM DEM was used to delineate the watershed. Disaster source analysis assessed the extent of land cover change in the watershed upstream zone. The results showed a significant land cover change in the downstream zone due to debris material covering an area of 9.86 ha. The affected land cover was a built-up area of moderate and low-density vegetation. A source zone was found, characterized by an extent increase of bare soil upstream of 5.48 ha.

Keywords: land cover, flash flood, mapping, remote sensing, GIS.

1. Introduction

Flash floods hit Simangulampe Village, Humbang Hasundutan District, North Sumatera Province, Indonesia, on December 1st, 2023, damaging buildings and built-up areas. The heavy rains increased the water discharge of the Sibuni-buni Creek, delivered mixed substances, and created debris flow. These materials also buried productive agricultural land and changed the surrounding environment. The impact of flash floods is reflected in the land cover change around the affected area.

Erosion and landslides are typical incidents strongly associated with flash floods. The displacement of materials eroded by water flow on steep slopes is a major trigger for flash floods. The runoff that occurred not only contained water but also carried various materials such as mud, stones, branches, wood, and all kinds of other heavy substances. Thus, it can significantly increase its kinetic energy and destructive forces to the surroundings [1]. Catane et al. [2] and Zain et al. [3] described some factors influencing this disaster's occurrence, i.e.,

* Email : wikanjaya@fis.unp.ac.id

slope, soil, and rainfall. Thoha et al. [4] and Wasis et al. [5] underlined that land cover influences flash flood vulnerability. Rumapea et al. [6] provided another perspective where the high precipitation (rainfall) is the most influential factor. Reinforcing that premise, Modric et al. [7] explained that the characteristics of the watershed also influence the probability of flash flood occurrence. These characteristics are categorized as morphometric parameters, constant channel maintenance, and perimeter of the watershed [8], [9]. Disaster impact assessment is one of the most critical parts of disaster emergency response. The impact quantity, location, and spatial extent are the primary information that must be inventoried in post-disaster management [10]. Principally, the impact of flash floods in specific areas could be determined by assessing land cover change before and after the calamity. The comparison of typical information could be conducted through a map, revealing its spatial distribution and allowing for a specific analysis of the impact [11].

Remote Sensing (RS), integrated with the Geographic Information System (GIS), has developed rapidly as a tool for monitoring and evaluating spatial phenomena, including disasters. The superiority of those technologies lies in their ability to continuously record images at the same location or at a specific time, allowing them to provide pre and post-disaster imagery [12]. The temporal resolution of satellite imagery allows for detecting changes due to disaster occurrence, whereas GIS could spatially analyze its impact.

Planet Scope is one of the most popular satellite imagery for multitemporal analysis. Roy et al. [13] explained that this imagery's advantage lies in its high spatial resolution of 3 m for the panchromatic and 8 m for the multispectral bands. The high spatial resolution enhances the accuracy of object identification. Additionally, the imagery provides eight multispectral bands, enabling more detailed spectral analysis through vegetation, greenness, and wetness index indices, thus improving analytical performance [14].

Moreover, Planet Scope is constantly recorded in a specific location daily [15], [16]; with this high temporal resolution, post-disaster impact analysis can be conducted quickly. This study uses RS and GIS to map land cover changes resulting from flash floods. Additionally, the source area of the flood is an essential aspect to be examined. Therefore, this research also analyzes the source location of flash floods.

2. Method

2.1. Location

The research was conducted in the Subuni-buni Watershed, Simangulampe Village, Batikraja District, Humbang Hasundutan Regency, North Sumatera Province of Indonesia. It is located between Longitude 98°49'33.152"E 2°19'8.927"N to 98°50'57.833"E 2°17'12.087"N (Figure 1**)**. This watershed was affiliated with the Asahan Toba Watershed system, which discharges water into the world's largest caldera, Lake Toba [17].

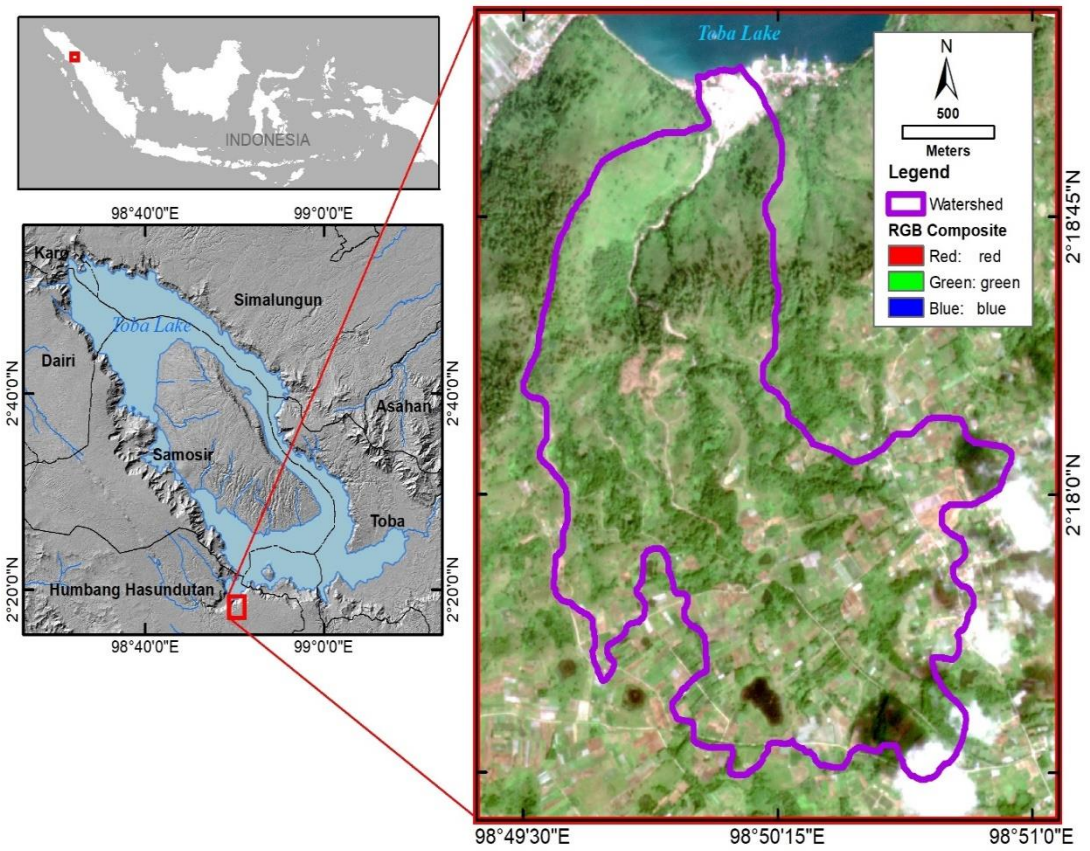

Figure 1: A satellite image of the study area location

Tectonically, the study area is part of the Toba Caldera Complex, formed during the Quaternary period through volcanic tectonic explosive processes [18]. It is located in the Great Sumatra Fault Zone (GSFZ), and the area is controlled by the Semangko Fault in the NW to SE direction [19], [20]. This complex comprises at least three calderas: Porsea, Haranggaol, and Sibandang. These calderas are identified based on their associated formations, i.e., the Old Toba Tuff (OTT) dating back to 0.84 Ma, the Middle Toba Tuff (MTT) at 0.501 Ma, and the Young Toba Tuff (YTT) at 0.074 Ma. Additionally, the Samosir dome, formed by the uplift of lava due to residual energy after the eruption, was also present. The Toba Tuff Formation (Qvt) dominates the study area, consisting of polymictic rhyo-dacitic rocks, heterolithic crystal-vitric ash-flow tuff, and a thin layer of airfall tuff. In the central zone of the caldera, the Samosir Formation (Qps) is composed of tuffaceous sandstone, siltstone, conglomerates, and diatomaceous materials. On the western slopes of the caldera rim, the Kluet Formation (Puk) is exposed and characterized by metaquartzose arenites, slates, and phyllites. Hanggono et al. [21] explain that the formation formed by volcanic tuff toba has a high amplification level and is vulnerable to mass movement due to seismic activity (Figure 2).

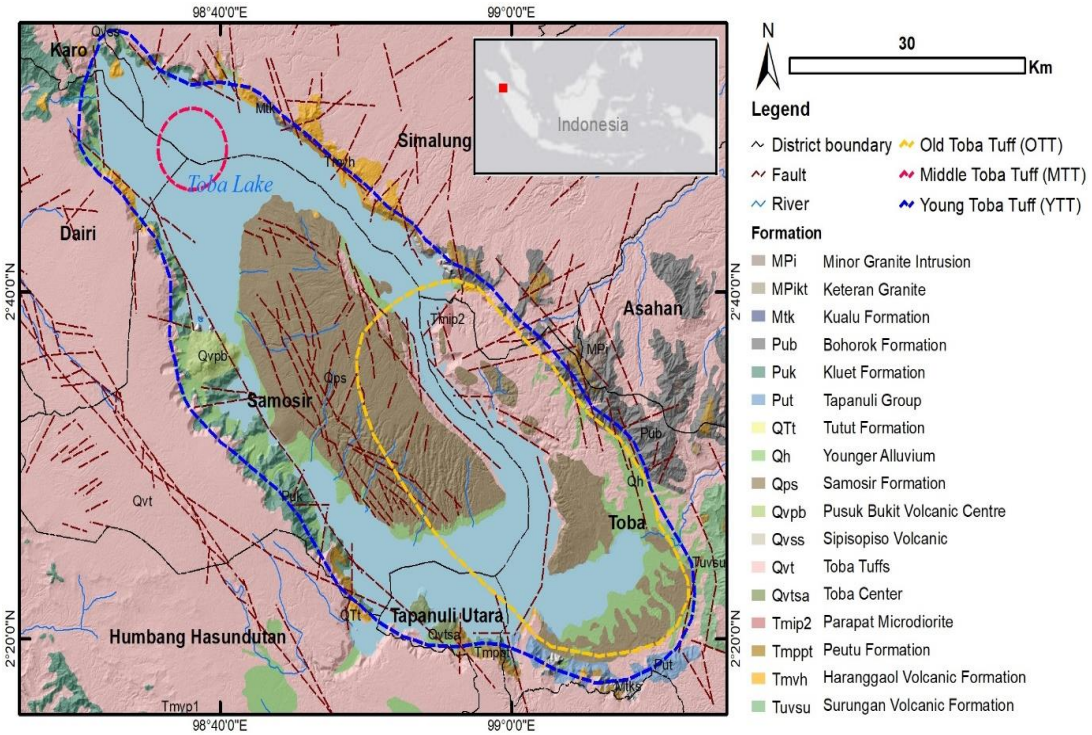

Figure 2: Geological setting of the study area

2.2. Watershed Interpretation

The first stage of this research was interpreting the watershed area as a boundary of the analysis unit. A 30 m resolution of Shuttle Radar Topography Mission (SRTM) Digital Elevation Model (DEM) data was utilized to obtain slope steepness and produce hill shade maps to define watershed and morphology zonation. The slope map was derived from a 3D slope analysis and classified according to Van Zuidam's classification. The slope classification is a proper categorization for mass movement analysis related to landslides and erosion. The hill shade model emphasizes topographic effects and encourages the identification of watershed boundaries. Watershed morphological zonation was identified from slope similarity and stream order reinforced with river maps produced by accumulation analysis using DEMDEM accumulation analysis.

2.3. Image Processing

Multitemporal Planet Scope imageries were implemented in this study to determine the land cover change due to the flood. This study utilized Planet Scope imageries recorded on November 08^{th,} 2023, as pre-disaster and December 8^{th,} 2023, as post-disaster images. The multitemporal Planet Scope imageries specifications are listed in Table 1.

Table 1: Planet Scope image specifications

Parameters	***Specifications***
Sensor type	Four-band frame imager with a split-frame VIS+NIR filter
Spectral bands	Blue: 455 – 515 nm Green: 500 – 50 nm Red: 590 – 670 nm NIR: 780 – 860 nm
Ground sample distance (nadir)	30 m – 4.1 m (approximate, altitude dependent)
Frame size	24 km x 16 km (approximate)
Revisit time (temporal resolution)	Daily at nadir

The initial image processing was conducted using radiometric and geometric correction. Radiometric correction was applied to improve the spectral quality of the imagery, whereas geometric correction resulted in positionally accurate imageries. The radiometric correction implemented in the data was digital number conversion into reflectance values using the coefficient contained in the imagery's metadata. This process was spectral calibration at the Top of the Atmosphere (TOA) reflectance level. On the other hand, the geometric correction applied was an image rectification method intended to equalize the positional accuracy of the two images.

The corrections were essential for analysis through image processing named multispectral classification. The land cover maps were generated from multispectral classifications employing a maximum likelihood algorithm for pre- and post-disaster imageries. Some Point of Interest (POI) samples were taken by selecting specific pixels representing land cover for each class object, i.e., high to low-density vegetation, water body, built-up area, and bare soil.

2.4. Land Cover Changes Analysis

The land cover change could be identified by overlaying land cover maps of pre- and post-flash flood occurrence. Each land cover class was calculated and analyzed using a confusion matrix. In addition to the quantitative analysis of land cover change, spatial analysis was applied by reviewing the geographical location of the land cover changes. Determination of the source and affected areas was conducted by analyzing land cover change and its spatial association with the watershed morphological zone.

3. Result

The delineation showed that the watershed of Sibuni-buni has an area of 487,83 ha. Morphologically, the watershed is divided into upper (upstream) zones of 240.05 ha, middle 230.77 ha, and lower (downstream) zones of 17.00 ha. Stream order was an indicator of watershed morphology. The first and second orders developed in the upper part, where permanent rivers had not been formed. In the middle part, the order develops massively, supported by a large level of slope difference. Downstream was where the highest river order was formed. It was indicated by the merging of all streams into a single stream. Zoning watershed morphology and slope class can be seen in Figure 3**.**

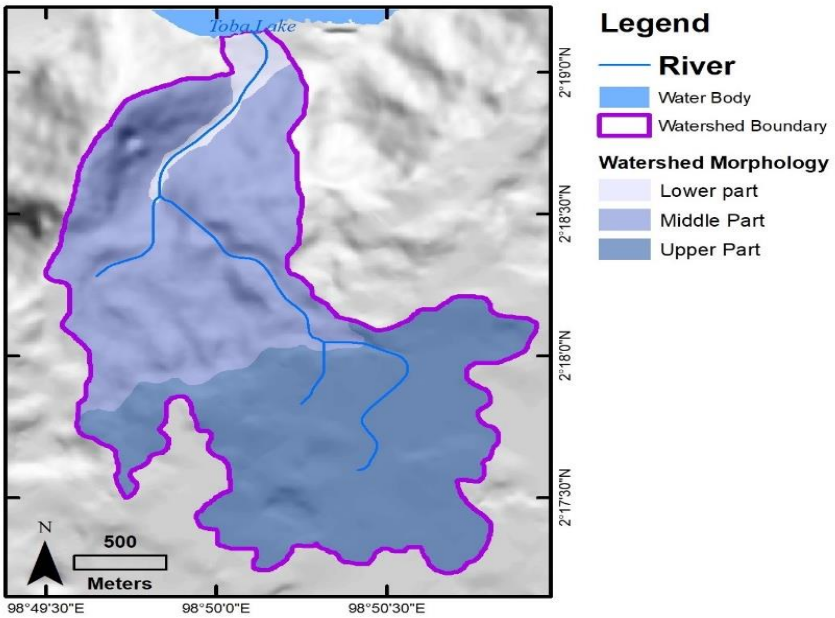

Figure 3: Watershed Morphology of Sibuni-buni Watershed

The main characteristic that controls the watershed morphology is the slope difference that forms the river gradient. The upper part was dominated by slopes between 4 to 8 degrees. The middle zone had a relatively more varied slope between 8 to 57 degrees. In those parts, the frequency of slope changes was considerable and had a relatively rough relief compared to the upstream and downstream. In contrast to both, the depositional section downstream was a zone with the dominance of the gentlest slopes, which ranged between 0 and 4 degrees, Figure 4.

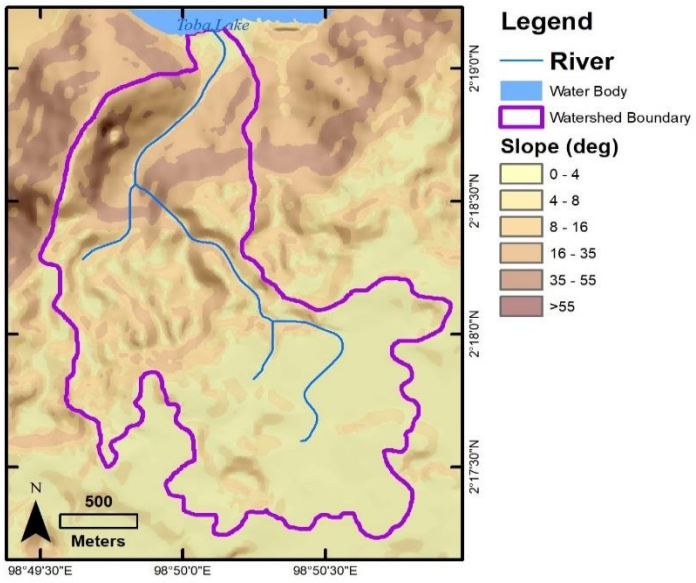

Figure 4: Slope class of Sibuni-buni Watershed

Pre-disaster land cover was dominated by low-density vegetation with an area of 144.85 ha, followed by medium and high-density vegetation with 129.94 ha and 122.86 ha (Figure 5). The area was mainly utilized as a production forest and mixed gardens. Bare soil has an area of about 82.21 ha, dominated by agricultural and unutilized land. The built-up area was the narrowest land cover, with an area of about 6.04 ha. Built-up land was distributed in the area around the downstream of the watershed. The area has intensive residential development because it is a tourist area with the main attraction of Lake Toba Beach.

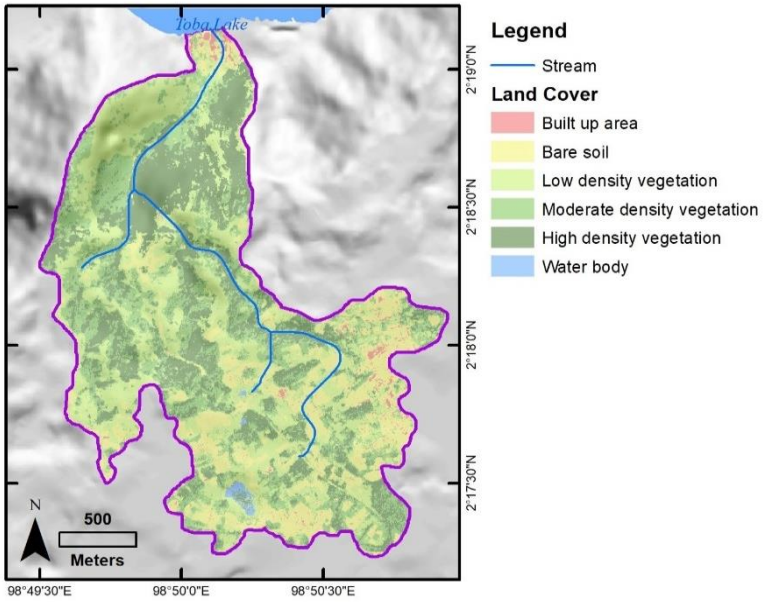

Figure 5: Land cover before the flash flood

The flash floods generally altered the study area's land cover, Figure 6. Spatially, these changes occurred in the middle zone and downstream (lower) part of the watershed.

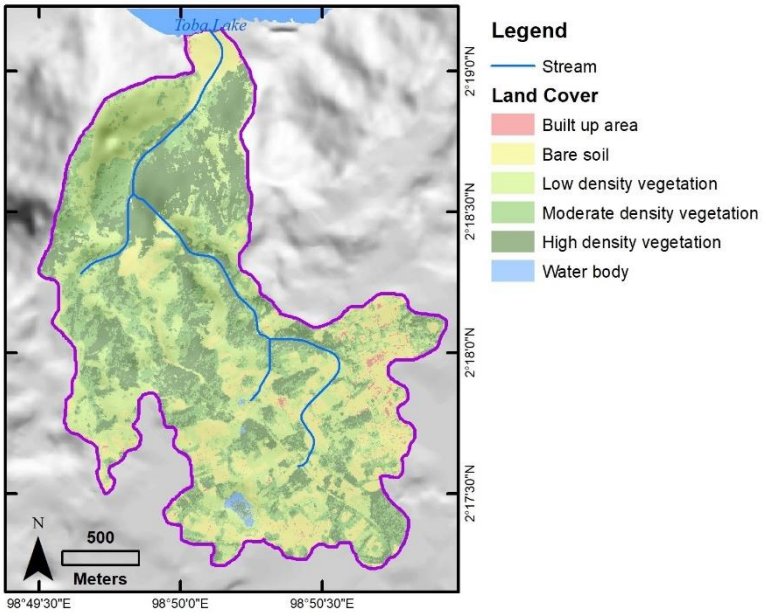

Figure 6: Land cover after flash flood

Bare soil became a land cover that experienced a large increase; at least the increase of bare soil was 8.96 ha or equivalent to 9.71% of the area before the flash flood. The expansion includes 1.76 ha of built-up area, 4.69 ha of low-density vegetation, 1.93 ha of moderate-density vegetation, and 0.57 ha of high-density vegetation, Table 2.

Table 2: Land cover change pre and post-flash flood

		Post-Flash Flood						
	Land Cover	**Built-Up Area**	**Bare Soil**	**Water Body**	**Low-Density Veg**	**Moderate Density Veg**	**High Density Veg**	**Total (ha)**
Pre-Flash Flood	**Built-Up Area**	4.27	1.76					6.04
	Bare Soil		82.21					82.21
	Water Body			1.93				1.93
	Low-Density Veg		4.69		140.16			144.85
	Moderate Density Veg		1.93			128.01		129.94
	High Density Veg		0.57				122.28	122.86
	Total (ha)	4.27	91.17	1.93	140.16	128.01	122.28	487.83

4. Discussion

Flash floods caused debris material to be transported by the run-off. The event was followed by deposition in the downstream area, previously dominated by built-up land cover and settlements. The resulting depositional material forms a colluvial fan. The form was characterized by unsorted material, such as large rocks, gravel, and sand, and tree trunks even accompanied it; the spatial distribution of land cover changes is shown in Figure 7.

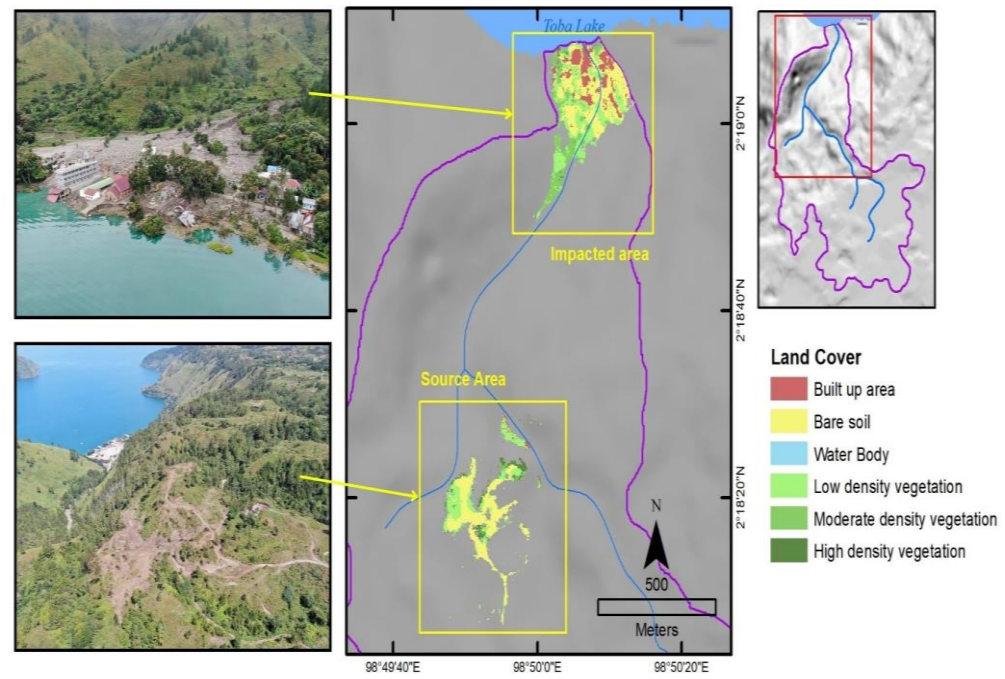

Figure 7: Flash flood impacted area and source area.

The effect was reflected by the skyrocketing extent of bare soil with 9.86 ha in the downstream area. Thus, these areas are then defined as flash flood-impacted areas. Based on the results of the analysis, the extent of the built-up area shrunk by 1.65 ha. In addition, low and medium-density vegetation utilized as agricultural land decreased by 2.76 ha and 1.72 ha. Details of the land cover affected by the flash flood are presented in Table 3.

Unlike the downstream zone, the central part of the watershed has an extent of increasing bare soil to 5.48 ha. It means that these areas lost land cover due to erosion and landslides. Previously, there was 2.90 ha of bare soil in that area. Low-density vegetation was eliminated with 1.74 ha, followed by high-density vegetation with 0.52 ha. This reduction was in line with the denudational process. This phenomenon occurred in the watershed with large relief roughness and dominant slopes between 35-55 deg. Based on the synthesis, the area was defined as the source of flash flood material or erosion-affected area (Table 3).

Table 3: Land cover change in source zone and affected zone

Land Cover	Source Area	Impacted Area
Bare soil	2.90	3.67
Built up area	0.12	1.65
High-density vegetation	0.52	0.06
Low-density vegetation	1.74	2.76
Moderate density vegetation	0.21	1.72
Total (ha)	5.48	9.86

The study of land cover dynamic changes in the area provides information on variations in quantity and spatial distribution. Using the morphological watershed approach can ease the task of separating the source and depositional or disturbed regions of a flash flood event. Comprehending land cover change data and this information's location adds essential and valuable information to the reconstruction programs after disasters.

5. Conclusion

Flash Flooding in the downstream zone of the Sibuni-buni watershed, Simangulampe, especially flash floods, has majorly altered land cover of around 9.86 ha. The area affected by the disaster was covered by built-up areas with moderate and low-density vegetation, and the principal use of land was covered by aggravated vegetation and agricultural lands. This debris material was collected from middle watershed morphological zones with a coverage of 5.48ha that had been greatly eroded. This is evidenced by the change in land use patterns whereby areas with low-density vegetation cover and bare ground were cleared.

6. Acknowledgments

The authors would like to acknowledge *Kelompok Studi dan Pengembangan Prakarsa Masyarakat* (KSPPM) for the permission to use the data and aerial photographs from their disaster investigation report. Aerial drone photos benefit this research as they provide valid and actual supporting data.

References

[1] A. Mukherjee, Md. Faisal, and M. K. Saha, "Measuring Resilience of Urban Slum to Climate-Induced Disasters: A Study on Barishal City Corporation, Bangladesh," *International Journal of Disaster Management*, vol. 3, no. 2, pp. 34–47, 2020.

[2] S. G. Catane, C. C. Abon, R. M. Saturday, E. P. P. Mendoza, and K. M. Futalan, "Landslide-amplified flash floods—The June 2008 Panay Island flooding, Philippines," *Geomorphology*, vol. 169–170, pp. 55–63, Oct. 2012.

[3] A. Zain, D. Legono, A. P. Rahardjo, and R. Jayadi, "Review on Co-factors Triggering Flash Flood Occurrences in Indonesian Small Catchments," *IOP Conf Ser Earth Environ Sci*, vol. 930, no. 1, p. 012087, 2021.

[4] A. S. Thoha, D. Sundari, P. Patana, and N. Sulistiyono, "Spatial distribution of landslide vulnerability level in Dairi District, North Sumatera Province, Indonesia," *J Phys Conf Ser*, vol. 1542, no. 1, p. 012011, May 2020.

[5] B. Wasis, D. Harlan, and M. H. W. Putra, "Impact of forest land cover on runoff, erosion and sedimentation in the Karai Watershed, Simalungun Regency, North Sumatra Province, Indonesia," *Archives of Agriculture and Environmental Science*, vol. 5, no. 1, pp. 40–49, Mar. 2020.

[6] H. Rumapea, M. Zarlis, P. Sihombing, S. Efendi, M. Sinambela, and I. J. A. Saragih, "Convective Cloud Classification Model for Reconstruction of Heavy Rain That Triggers the Flood and Landslide in Parapat, North Sumatera," *IOP Conf Ser Earth Environ Sci*, vol. 1083, no. 1, p. 012017, Sep. 2022.

[7] T. M. Modrick and K. P. Georgakakos, "The character and causes of flash flood occurrence changes in mountainous small basins of Southern California under projected climatic change," *J Hydrol Reg Stud*, vol. 3, pp. 312–336, 2015.

[8] P. Raja Shekar and A. Mathew, "Morphometric analysis of watersheds: A comprehensive review of data sources, quality, and geospatial techniques," *Watershed Ecology and the Environment*, vol. 6, pp. 13–25, 2024.

[9] M. Y. I. Kurzah, N. Nurhayati, and E. Yulianto, "Morphology and Morphometry Characteristic of Raya Watershed," *Jurnal Teknik Sipil*, vol. 24, no. 1, p. 839, Apr. 2024.

[10] N. Yeşiller *et al.*, "Disaster reconnaissance framework for sustainable post-disaster materials management," *Waste Management*, vol. 169, pp. 392–398, Sep. 2023.

[11] D. Pratiwi, D. Putri, R. Syamsul Arif, J. A. Kartika, C. Riski Fathurohman, and D. Apriyanti, "Identification and Analysis of Landslide Soil Vulnerability as The Basis of Disaster Mitigation with Geodetic Measurement Methods and Quantitative Description," *BulletinOfGeology*, vol. 6, no. 2, p. 2022, 2022.

[12] J. Barnetson, S. Phinn, and P. Scarth, "Mapping woody vegetation cover across Australia's arid rangelands: Utilising a machine-learning classification and low-cost Remotely Piloted Aircraft

System," *International Journal of Applied Earth Observation and Geoinformation*, vol. 83, p. 101909, Nov. 2019.

[13] D. P. Roy, H. Huang, R. Houborg, and V. S. Martins, "A global analysis of the temporal availability of PlanetScope high spatial resolution multi-spectral imagery," *Remote Sens Environ*, vol. 264, p. 112586, Oct. 2021.

[14] E. A. W. A. Putri, P. Danoedoro, and N. M. M. Farda, "Comparing land-cover maps accuracies generated from multispectral classification of Landsat-8 OLI dan Pleiades images using two different classification schemes," in *Sixth Geoinformation Science Symposium*, Yogyakarta, Nov. 2019.

[15] H. Huang and D. P. Roy, "Characterization of Planetscope-0 Planetscope-1 surface reflectance and normalized difference vegetation index continuity," *Science of Remote Sensing*, vol. 3, p. 100014, Jun. 2021.

[16] A. S. Sesama, K. T. Setiawan, and A. Julzarika, "Bathymetric Extraction Using Planetscope Imagery (Case Study: Kemujan Island, Central Java)," *International Journal of Remote Sensing and Earth Sciences (IJReSES)*, vol. 17, no. 2, p. 209, 2021, doi: 10.30536/j.ijreses.2020.v17.a3445.

[17] R. W. Fairbridge, "Lake toba," in *Geomorphology*, Dordrecht: Kluwer Academic Publishers, pp. 617–618.

[18] C. A. Chesner, "The Toba Caldera Complex," *Quaternary International*, vol. 258, pp. 5–18, May 2012.

[19] I. Koulakov *et al.*, "The feeder system of the Toba supervolcano from the slab to the shallow reservoir," *Nat Commun*, vol. 7, no. 1, p. 12228, Jul. 2016.

[20] S. Liu, I. Suardi, X. Xu, S. Yang, and P. Tong, "The Geometry of the Subducted Slab Beneath Sumatra Revealed by Regional and Teleseismic Traveltime Tomography," *J Geophys Res Solid Earth*, vol. 126, no. 1, Jan. 2021.

[21] T. Anggono *et al.*, "Microzonation study around Lake Toba, North Sumatra, Indonesia based on horizontal – vertical spectral ratio," *IOP Conf Ser Earth Environ Sci*, vol. 1233, no. 1, p. 012023, Aug. 2023.